Geophysical Journal International

*Geophys. J. Int.* (2020) **223,** 444–453
Advance Access publication 2020 June 27
General Geophysical Methods

doi: 10.1093/gji/ggaa322

# Optimized approximate inverse Laplace transform for geo-deformation computation in viscoelastic Earth model

He Tang, Lan Zhang, Le Chang and Wenke Sun

*Key Laboratory of Computational Geodynamics, University of Chinese Academy of Sciences, Beijing* 100049*, China. E-mail: sunw@ucas.ac.cn*

Accepted 2020 June 24. Received 2020 June 24; in original form 2020 April 29

## SUMMARY

Integral transformations, especially the inverse Laplace transform, are powerful techniques for resolving a wide range of geophysical and geodynamic simulation problems in viscoelastic materials. The exact location or distribution range of poles of the image function in a complex plane is usually necessary for applying numerical algorithms such as contour integration. Unfortunately, there are innumerable poles (such as those of post-seismic deformations) in a realistic Earth model with continuous stratification, finite compressibility and self-gravitation. Here, an optimized method to effectively calculate the inverse Laplace transform is presented. First, the integral kernel is approximated as a rational function with two parameters ($a$ and $m$). Thereafter, the residue theorem is analytically applied to the approximated integrand. Finally, a series formula of the inverse Laplace transform sampling of image functions along a contour line parallel to the image axis is obtained. The proposed approximate scheme of the inverse Laplace transform is discussed by some common geophysical signals and the optimized selection of two parameters ($a = 6$ and $m = 4$) is conducted after a detailed analysis. The proposed method is anticipated as being able to help performing certain theoretical studies related to geodynamic problems with viscoelastic deformations.

**Key words:** Creep and deformation; Loading of the Earth; Seismic cycle; Numerical approximations and analysis; Rheology: mantle.

## 1 INTRODUCTION

The Earth behaves as a perfectly elastic solid body under short-term geodynamic processes (those that occur in seconds to minutes), such as seismic wave propagation. Its anelasticity, however, also performs an essential function for certain long-term (occurring over weeks to millions of years) geophysical and geodynamic processes—such as post-seismic deformations, postglacial rebound and mantle convection. These longer processes involve interactions between the elastoplastic crust and viscoelastic mantle and result in global or regional geophysical deformations.

To accurately model these spatio-temporal deformations induced by earthquakes and post-glacial rebound, anelasticity, particularly the upper mantle's viscoelastic property, should be considered. To simulate the geo-deformations in the Earth model, which is usually a spherical viscoelastic model, differential equations in time and space domains typically require accurate solutions. Among the most common techniques employed to effectively solve these equations are spatio-temporal finite-difference algorithms, basic function expansions and integral transformations.

Two of these approaches—basic function expansions and integral transformations—even yield some semi- or fully analytical solutions in the transformed mathematical domain or even in the real physical space for certain problems. For example, the exact solution of Boussinesq problem is obtained through the Hankel transform (Farrell 1972). Moreover, to investigate the viscoelastic or elastic deformations in a spherically symmetric Earth model, the semi-analytical Love number framework is employed (Farrell 1972; Pollitz 1992; Sun & Okubo 1993, 2002; Piersanti *et al.* 1995; Pollitz 1997; Spada & Boschi 2006; Tanaka *et al.* 2006, 2007; Tang & Sun 2019). The integral transform contains two parts: the forward and inverse transforms. The forward transform, which is a relatively simple and clear process, is usually applied analytically to differential equations to convert the problem into a simple and known form. The inverse transform can only be achieved in analytical form in a simple Earth model (e.g. Tang & Sun 2018; Tang *et al.* 2020), but it can be approximately calculated by a numerical scheme in a more realistic Earth model.

The forward and inverse Laplace transforms are commonly used mathematical approaches to geodynamic simulation of viscoelastic material. All theoretical studies that investigate seismic viscoelastic deformations involve the use of an inverse Laplace transform. For example, the simulation of post-seismic deformations via normal mode uses an analytical inverse transform (Sabadini *et al.* 1984; Pollitz 1997). A transform based on a closed-path integration method employs a numerical inverse Laplace integration (Tanaka *et al.* 2006, 2007). A transform built on Post's inversion formula,

which applies a weighted summation of specifically sampled complex functions (Melini *et al.* 2008), is essentially a numerical variant of the inverse transform.

The main hindrance in some algorithms of the inverse Laplace transform is the necessity for a prior distribution of poles in the complex plane. This oscillational inverse Laplace integration should be handled carefully with a dense sampling scheme. The poles in the complex plane differ because of specific problems and are strongly dependent on the viscoelastic Earth model in terms of stratification structure, compressibility, self-gravitation, rheological structure and source type. Locating the positions of all poles or estimating the distribution range of poles is a key step for the inverse transform. The oscillational property of inverse Laplace transform may not exert a extremely detrimental influence on common calculations if a suitable numerical integration with sufficient accuracy is employed; however, this results in low computational efficiency and inconvenient accessibility.

There are different approaches to resolve the foregoing problems. The normal mode method was first achieved by some scientists as a semi-analytical method (Piersanti *et al.* 1995; Pollitz 1997; Vermeersen & Sabadini 1997). With this technique, numerous layers (from several dozens to a hundred) can be considered within an incompressible Earth model. Additionally, the normal mode summation within semi-analytical method can be also used for compressible Earth model, as shown by Cambiotti *et al.* (2009, 2013) and Cambiotti & Sabadini (2010). The normal mode approach has a definite value for determining the contribution of each mode to the final deformations and should not be disregarded in certain studies. In fact, this method has been widely used in practical applications, such as the modelling of the viscoelastic deformation with Maxwell or Burgers rheology (e.g. Ozawa *et al.* 2011) or the estimate of the viscosity profile by multiple geodetic observations (e.g. Pollitz *et al.* 2006). For this method, however, a highly accurate but computationally difficult root-finding algorithm is necessary. Moreover, when continuous stratification and compressibility are simultaneously considered, the normal mode method is beset by the difficulty of numerically searching for innumerable poles in the realistic Earth (Vermeersen *et al.* 1996; Tanaka *et al.* 2006; Cambiotti *et al.* 2009; Cambiotti & Sabadini 2010; Tang & Sun 2019).

By avoiding the search for poles in the inverse Laplace transform, new approaches for reducing the amount of calculation may be formulated. This may possibly extend the use of the transform to a more realistic Earth model and to make it more suitable for inverse problems. As stated by Spada & Boschi (2006), the root-finding procedure and Bromwich integral can be bypassed if the normal mode formulation is suitably modified by applying the Post–Widder inverse Laplace formula. Melini *et al.* (2008) subsequently successfully achieved various benchmarks using a Fortran 90 multiprecision library to tune this algorithm. They concluded that this method is highly accurate for modelling post-seismic deformations on a realistic Earth model with complex Maxwell and Burgers rheologies. Other algorithms, such as the numerical inverse fast Fourier transform applied by Wang *et al.* (2006), are also proven effective.

Recently, Tang & Sun (2019) confirmed that an approximate kernel approach (Valsa & Brancik 1998) is also applicable for simulating the post-seismic deformation in a realistic Earth model with a complex stratification structure and rheology profile. In essence, their method is to make an approximation of the integral kernel in the inverse transform, and the approximation degree of the integral kernel will affect the convergence speed and calculation error of this algorithm. A better approximation of the integral kernel should give more accurate results, but it may lead to a decrease in convergence speed. Therefore, the speed of convergence and the accuracy of calculation needs to be taking into account in a trade-off view. After the publication of the above paper, we think deeply about the idea of integral kernel approximation and find that a better approximate kernel can be achieved, keeping a good convergence at the same time. It is found that there is extra space available to further improve through concentrating on the main nature of the problem and simplifying the mathematical process. In other words, the parameters of this approximation approach should be generalized and optimized. This is the motivation for extending the previous study to achieve a better approximate inverse Laplace transform in studying for viscoelastic geo-deformation. Moreover, the improved method could be considered as a common technique that may be extended so that it can be employed for other similar problems.

In the following section, a general approximate inverse Laplace transform approach is first proposed; thereafter, its validity is verified. A parameter selection guide and an application example are also provided.

## 2 APPROXIMATE METHOD FOR INVERSE LAPLACE TRANSFORM

### 2.1 Method principle

The detailed mathematical derivation process is presented in Sections 2.1 and 2.2; a summary is provided in Section 2.3 for those not interested in these derivations.

The Laplace transform of a real function, $f(t)$, is defined as

$$F(s) = \int_0^{+\infty} \mathrm{e}^{-st} f(s)\, dt\ , \mathrm{Re}(s) > \alpha. \tag{1}$$

The function $f(t)$ is usually referred to as the original function and $F(s)$ is the corresponding image function. To ensure the convergence of the integral, it is assumed that $f(t)$ is continuous and of an exponential order, $\alpha$, that is $|f(t)| \leq M\mathrm{e}^{\alpha t}$ with $M > 0$ and $\alpha \geq 0$. The inverse Laplace transform of $f(t)$ is then given by the Bromwich integral as follows:

$$f(t) = \frac{1}{2\pi i} \int_{c-i\infty}^{c+i\infty} F(s)\, \mathrm{e}^{st} ds. \tag{2}$$

Here, $c$ is chosen to be larger than $\alpha$, that is the vertical contour in the complex plane retains all singularities of $F(s)$ on its left. A new strategy to handle this oscillatory infinite integral (eq. 2) is presented by approximating the integral kernel and implementing the residue theorem. The approximation of integral kernel $\mathrm{e}^{st}$ along the integration path (Valsa & Brancik 1998; Tang & Sun 2019) can be written in a new form with two parameters, $a$ and $m$, as below:

$$\mathrm{e}^{st} \approx \frac{\mathrm{e}^{st}}{1 - \mathrm{e}^{-m(a-st)}},\ \mathrm{e}^{-m(a-ct)} \ll 1. \tag{3}$$

The second part of eq. (3) ensures a sufficiently good approximation of the integral kernel. Note that if the negative sign of the exponential term in the denominator of eq. (3) is made positive, then the resulting expression will be the same as eq. (7). The above approximation expression can be treated as a general form of the original one used by Valsa & Brancik (1998), that is the expression $\mathrm{e}^{-2(a-st)}$ is extended as $\mathrm{e}^{-m(a-st)}$ with an additional parameter $m$. It is foreseeable that when $m$ is greater than 2, the above expression has a better approximation effect and may lead to a smaller calculation error. However, $m$ cannot be infinitely large, because when $m$ is infinitely large, the approximation strategy will fail. So, the parameters of eq. (3) should be optimized which will be discussed later. It is clear that

both the two parameters $a$ and $m$ are real numbers from their definitions. Nevertheless, to reduce the complexity of analysing without losing the guidance of choosing their approximate values, the two parameters will be optimal constrained in the integer number filed instead of the real number field by some numerical calculations.

The inverse Laplace transform of $F(s)$ is approximated as below (also see Fig. 1):

$$f(t) \approx f_{am}(t) = \frac{1}{2\pi i}\int_{c-i\infty}^{c+i\infty} G(s)\,e^{st}ds, \qquad (4)$$
$$G(s) = \frac{F(s)}{1-e^{-m(a-st)}}, e^{-m(a-ct)} \ll 1.$$

That is, the inverse Laplace transform of $F(s)$ is approximated by that of $G(s)$. To calculate the transform of $G(s)$, another curve integral along the semi-circle with an infinite radius ($R$) and the centre at ($c$, 0) is added to obtain a closed path integral. Because $F(s) \to 0$ as $s \to \infty$, $G(s) \to 0$ as $s \to \infty$. It can be assumed that $|G(s)| \le \varepsilon$, where $\varepsilon$ is a positive variable for a large $|s|$. First, the curve integral ($f_{ACB}$) along arc ($\widehat{ACB}$) is estimated as follows:

$$\begin{aligned}|f_{ACB}| &= \left|\int_{\widehat{ACB}} G(s)\,e^{st}ds\right| \le \varepsilon\int_{\widehat{ACB}}\left|e^{st}\right||ds| \\ &= \varepsilon\int_{-\pi/2}^{\pi/2} e^{t(c+R\cos\theta)}Rd\theta \le 2R\varepsilon e^{tc}\int_0^{\pi/2} e^{-2Rt\theta/\pi}d\theta \\ &\le \frac{e^{tc}\pi\varepsilon}{t}. \end{aligned} \qquad (5)$$

The above inequality is essentially that of Jordan's Lemma rotated through $\pi/2$. The integral can be as small as desired because $t > 0$ and $c$ is fixed, resulting in $f_{ACB}$ approaching zero as $R \to +\infty$. The residue theorem can thus be utilized for the closed path integral of $f_{am}(t)$.

For simplicity, the variables are defined as $P(s) = F(s)e^{st}$ and $Q(s) = 1 - e^{-m(a-st)}$. It is evident that these two complex functions are analytic in the complex plane and expected at some special points, $q_k$, of $Q(s)$; moreover, $P(q_k) \ne 0$, $Q(q_k) = 0$ and $Q'(q_k) \ne 0$. Eq. (4) is therefore rewritten as

$$\begin{aligned}f_{am}(t) &= -\sum_{k=-\infty}^{+\infty}\mathrm{Res}(P/Q, q_k) \\ &= -\sum_{k=-\infty}^{+\infty}\left(P/Q'\right)\big|_{s=q_k}, \mathrm{Re}(q_k) > c. \end{aligned} \qquad (6)$$

The zero point of $Q(s)$ is $q_k = (am - 2k\pi i)/mt$ with $k \in Z$. Here, $Q'$ denotes the derivative of $Q(s)$.

After some simple algebraic operations, eq. (6) can be written as

$$\begin{aligned}f_{am}(t) &= \frac{e^a}{mt}\sum_{k=-\infty}^{+\infty} e^{-i\pi 2k/m}F\left(\frac{a}{t} - \frac{i\pi 2k}{mt}\right) \\ &= \frac{e^a}{mt}\left[2\sum_{k=0}^{+\infty} F\left(\frac{a}{t} + \frac{i2k\pi}{mt}\right)e^{i2k\pi/m} - F\left(\frac{a}{t}\right)\right] \end{aligned} \qquad (7)$$

$a/t > c$.

The above formula holds if $k$ is replaced by $-k$ because $F(s^*) = F^*(s)$, where $*$ denotes a conjugate operator. Note that the foregoing formula will yield a real value variable although it involves complex expressions in theory.

To achieve a satisfactory approximation of $f(t)$ by $f_{am}(t)$, suitable values of the parameter should be selected in the proposed method. The following conditions should be considered: $e^{-m(a-ct)} \ll 1$ and $a/t > c > \alpha$; $\alpha$ should be larger than all the real parts of the singularities of $F(s)$. The maximum value of the real parts of the singularities of $F(s)$ is $c_{\max}$. The conditions are simplified as follows: (1) $m \gg 0$ and $a/t > c_{\max}$, or (2) $m > 0$ and $a/t \gg c_{\max}$.

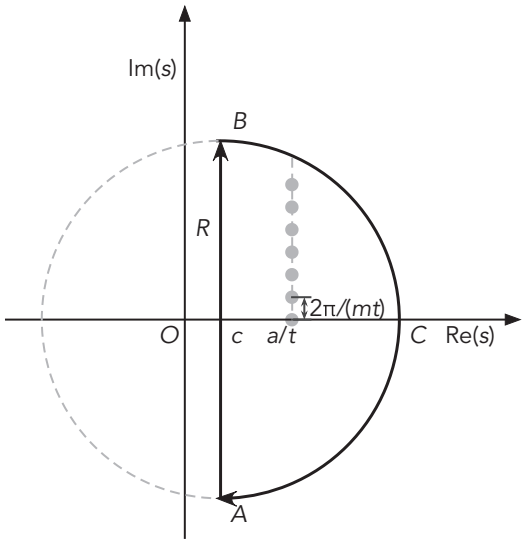


**Figure 1.** Sketch of proposed method for inverse Laplace transform. The black solid line is the new integration path containing a vertical line, Re($s$) = $c$, and a semi-circle, $\widehat{BCA}$, with radius $R$. The grey dots denote the poles of the approximate integrand with a shared real part, $a/t$, and a constant vertical step, $2\pi/(mt)$, for the imaginary parts (the poles below the Re(s) axis are omitted for symmetry).

In the actual calculation, the above series approximation of $f(t)$ may be truncated with a sufficient term and some series acceleration techniques may be employed to expedite convergence. The truncated series formula at $k = N$ is written as $f_{amN}(t)$ in the following subsection; the error estimation of the proposed method is also discussed.

### 2.2 Error analysis and acceleration scheme

The proposed inverse Laplace transform encounters errors emanating from (i) the approximation of the integration kernel and (ii) the truncation and acceleration of the series.

According to Valsa & Brancik (1998), the former can be called static error. The approximation of may be rewritten as

$$\begin{aligned}e^{st} &\approx \frac{e^{st}}{1-e^{-m(a-st)}} = e^{st} + e^{st}\sum_{k=1}^{+\infty} e^{-mk(a-st)} \\ &= e^{st} + \sum_{k=1}^{+\infty} e^{-amk}e^{s(mk+1)t}. \end{aligned} \qquad (8)$$

The approximate form of $f(t)$ is

$$\begin{aligned}f_{am}(t) &= \frac{1}{2\pi i}\int_{c-i\infty}^{c+i\infty} F(s)\left(e^{st} + \sum_{k=1}^{+\infty} e^{-amk}e^{s(mk+1)t}\right)ds \\ &= f(t) + \sum_{k=1}^{+\infty} e^{-amk}f(mkt+t). \end{aligned} \qquad (9)$$

The relative static error can be written as

$$\begin{aligned}\delta_S &= \left|\frac{f_{am}(t) - f(t)}{f(t)}\right| = \left|\sum_{k=1}^{+\infty} e^{-kma}\frac{f(mkt+t)}{f(t)}\right| \\ &\le \sum_{k=1}^{+\infty} e^{-kma}\left|\frac{f(mkt+t)}{f(t)}\right| \approx e^{-ma}\left|\frac{f(mt+t)}{f(t)}\right|. \end{aligned} \qquad (10)$$

For the geophysical problem, the deformation system is usually not an exponential divergence, but an exponential convergence. It can be conservatively assumed that for all types of geophysical signals, $\max\{|f(mt+t)|,\ m = 1, \ldots, +\infty\} \approx |f(t)|$ at any time

```
% Prepare weight
a = abs(a);
n = numel(a);
k = (1:n)';
p = 1/2;
Q = (n-k+1)./k;
d = exp(cumsum([n*log(p); log(Q)]));
w = cumsum(d);

% Alternate signs
a = a(:);
a(2:2:n) = -a(2:2:n);

% Reverse order
a = a(n:-1:1);

% Weighted sum
s = sum(w(1:n).*a)/w(n+1);
% Relative error
er = 2^(-n);
```

**Figure 2.** MATLAB code of a linear acceleration method, that is Euler's transform. The weighted sum ($s$) with a relative error (er $= 1/2\text{^}N$) is the series approximation of $\sum_{n=0}^{+\infty}(-1)^n A_n$ using the first $N$ terms of $A_n$ with $A_n \geq 0$. a denotes $A_n$ (lines that begin with ' per cent' are comment lines).

$t$. With this assumption, the relative static error can therefore be approximately written as

$$\delta_S = \mathrm{e}^{-ma} \approx 10^{-0.434ma}. \tag{11}$$

The second error source (i.e. series truncation and acceleration) depends on the number of terms and type of series acceleration technique employed. It is thus difficult to obtain an accurate estimation. Here, a common linear acceleration method, Euler–Van Wijngaarden transformation, also known as Euler's transform, is employed. The MATLAB code of Euler's transform is given in Fig. 2. This method's algorithm is relatively simple but considerably powerful.

To use this acceleration scheme, eq. (7) should first be rewritten as an alternating series

$$f_{am}(t) = \frac{\mathrm{e}^a}{mt}\left[2\sum_{n=0}^{+\infty}(-1)^n A_n - F\left(\frac{a}{t}\right)\right]. \tag{12}$$

In the foregoing, $A_n$ is a re-integration of the series in eq. (7) with the following constraint:

$$\sum_{n=0}^{+\infty}(-1)^n A_n = \sum_{k=0}^{+\infty}\mathrm{Re}\left[F\left(\frac{a}{t}+\frac{i2k\pi}{mt}\right)\mathrm{e}^{i2k\pi/m}\right], \tag{13}$$
$$A_n \geq 0.$$

The re-integration of the original series into one that is alternating is relatively easy because the exponential factor periodically changes its signal, and $F(s)$ is usually a well-behaved decay function.

It is assumed that a good approximation, $f_{amN}(t)$, of the infinite series in eq. (12) can be obtained by the first $N$ values of $A_n$; the algorithm can then be described by the MATLAB code in Fig. 2. As a simple estimation, the relative error of $f_{amN}(t)$ as a discrepancy from $f_{am}(t)$ is approximately

$$\delta_N = \frac{1}{2^N} \approx 10^{-0.301N}. \tag{14}$$

The proposed inverse Laplace transform method is thus considered as having a relative error of approximately

$$\delta = \max\{\delta_S, \delta_N\} \approx 10^{-\min\{0.434ma,\ 0.301N\}}, \tag{15}$$

where $\{a,\ m\}$ are the parameters of the proposed method, and $N-1$ is the truncation of the alternating series after re-integration.

### 2.3 Summary of proposed method

If the Laplace transform of a given function, $f(t)$, is written as $F(s)$, then its approximate inverse Laplace transform can be calculated with finite terms by

$$f_{amN}(t) = \frac{\mathrm{e}^a}{mt}\left[2\sum_{n=0}^{N-1}(-1)^n A_n - F\left(\frac{a}{t}\right)\right], \tag{16}$$
$$m \gg 0,\ a/t > c_{\max}$$

($c_{\max}$ denotes that the pole of $F(s)$ has the largest real part) with a re-integration of series $F(s_k)$ into an alternating series with the following constraint:

$$\sum_{n=0}^{+\infty}(-1)^n A_n = \sum_{k=0}^{+\infty}\mathrm{Re}\left[F\left(\frac{a}{t}+\frac{i2k\pi}{mt}\right)\mathrm{e}^{i2k\pi/m}\right], \tag{17}$$
$$A_n \geq 0.$$

To accelerate the series convergence, Euler's transform is applied.

The principle of this method is relatively clear and easy to understand, that is a weighted sum of the transformed function, $F(s)$, sampled along a vertical line in complex plane has a good approximation of its inverse Laplace transform. The parameters are all geometrically defined to establish the sampling scheme of the transformed function. The sampling points share the real part, $a/t$, and the two neighbouring points are separated by the distance $2\pi/(mt)$.

The relative error of this method is approximately

$$\delta = \max\{\delta_S,\ \delta_N\} \approx 10^{-\min\{0.434ma,\ 0.301N\}}. \tag{18}$$

The first term results from the approximation of the integration kernel and the second is caused by the truncation of the alternating series at $n = N-1$ after the series re-integration and Euler's transform acceleration. Here, $N$ is the total number of terms used for the alternating series as a re-integration of the series of $F(s_k)$. It is therefore dependent on the transformed function, $F(s)$, and the expected precision of the inverse transform.

Eq. (18) may be employed to estimate the suitable values of parameters $\{a, m\}$ depending on the expected precision and particular decay performance of a given $F(s)$. Note that the relative error estimate provided here is merely an approximation, and the parameter values are employed simply to check the actual results of specific problems. A detailed discussion on the choice of these two parameters, the validity of the relative error estimation, and the performance of the proposed method on common geophysical signals, is presented in the following section.

## 3 VALIDATION AND NUMERICAL TEST OF PROPOSED METHOD

### 3.1 Confirmation of validity using an exponential function

To check the above formulae (eqs 16–18), the exponential function $h(t)$ is used as an example:

$$h(t) = \mathrm{e}^{-t/\tau_0}, \tag{19}$$

whose Laplace transform is

$$H(s) = \frac{1}{s+1/\tau_0}. \tag{20}$$

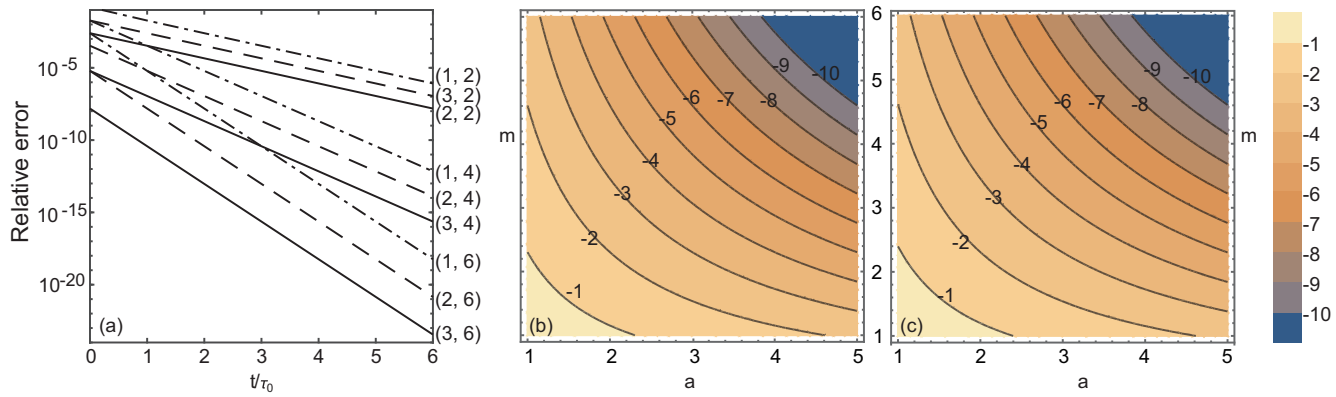


**Figure 3.** Relative error analysis of $h_{am}(t)$ with time $t$ and parameters $\{a, m\}$ change. (a) Relative error of $h_{am}(t)$ with different values of $\{a, m\}$; (b) relative error of $h_{am}(t = 0)$ obtained using the exact formula eq. (26); (c) relative error of $h_{am}(t = 0)$ obtained using the approximate error formula eq. (11). Each line in (a) is marked by the numbers on the right $(a_i, m_i)$. The contour lines in (b) and (c) are marked by $--j$, indicating that $10^{-j}$ is the relative error.

**Table 1.** Four signals in time domain and image functions in Laplace domain.

| Functions in the time domain | Functions in the Laplace domain |
|---|---|
| $f_1 = \mathrm{e}^{-t/\tau_0}$ | $F_1 = \frac{1}{s+1/\tau_0}$ |
| $f_2 = \sin(\omega_0 t)$ | $F_2 = \frac{\omega_0}{s^2+\omega_0{}^2}$ |
| $f_3 = \cos(\omega_0 t)$ | $F_3 = \frac{s}{s^2+\omega_0{}^2}$ |
| $f_4 = 3f_1 + 2f_2 + f_3$ | $F_4 = 3F_1 + 2F_2 + F_1$ |

The approximate inverse Laplace of $H(s)$ using eq. (7) is

$$h_{am}(t) = \frac{\mathrm{e}^a}{mt}\left[2\sum_{k=0}^{+\infty} H\left(\frac{a}{t} + \frac{i2k\pi}{mt}\right)\mathrm{e}^{i2k\pi/m} - H\left(\frac{a}{t}\right)\right]. \tag{21}$$

The sum of the infinite series can be analytically written as

$$h_{am}(t) = \frac{i\mathrm{e}^a}{2\pi}\left[\frac{{}_2HF_1\left(1, 1-x, 2-x, \mathrm{e}^{2\pi i/m}\right)}{x-1} + \frac{{}_2HF_1\left(1, x, 1+x, \mathrm{e}^{-2\pi i/m}\right)}{x}\right], \tag{22}$$

where $x = \frac{im}{2\pi}(a + t/\tau_0)$, and ${}_2HF_1(a, b, c, z)$ is the hypergeometric function. When $m = 2$, $h_{am}(t)$ may be written, after simplification, as follows:

$$h_{a2}(t) = \frac{\mathrm{e}^{-t/\tau_0}}{1 - \mathrm{e}^{-2(a+t/\tau_0)}}. \tag{23}$$

It is then easily proven that

$$\lim_{a\to+\infty} h_{a2}(t) = \mathrm{e}^{-t/\tau_0} \equiv h(t). \tag{24}$$

It can in fact be proved that

$$\lim_{a\to+\infty} h_{am}(t) \equiv h(t). \tag{25}$$

This confirms the validity of the proposed method if a suitable parameter, $a$, is chosen.

With the given values of parameters $a$ and $m$, there will be a discrepancy between the approximate formula, $h_{am}(t)$, and the exact one, $h(t)$. With the relative error $h_{am}^{RE}(t)$ of the approximate formula is

$$h_{am}^{RE}(t) = \left|\frac{h_{am}(t)}{h(t)} - 1\right|. \tag{26}$$

The relative error for $h_{am}(t)$ with different parameters $\{a, m\}$ are calculated and plotted in Fig. 3. The relative errors with different parameters $\{a, m\}$ exhibit a decay in performance over $t/\tau_0$ as shown in Fig. 3(a). In Figs 3(b) and (c), the relative errors of $h_{am}^{RE}(t = 0)$ are calculated by the exact formula eq. (26) and the approximate formula eq. (18), respectively. The contour line maps in Figs 3(b) and (c) exhibit good agreement. It indicates the proposed approximate algorithm of the inverse Laplace transform is valid.

The relative error in Fig. 3 shows that when large parameter values of $a$ and $m$ are chosen, the errors are small. Parameters $a$ and $m$ have practically the same effects on the relative error. The relative error can be made sufficiently small when an appropriately large value of $a \cdot m$ is employed.

### 3.2 Suggestions on parameter selection for certain geophysical signals

Section 3.1 above presents the checking of the approximate formulae of the inverse Laplace transform and static error estimation via an exponential function. This subsection presents the analysis of the performance of the proposed method, that is the accelerated series summation of $F(s_k)$ sampling along a chosen vertical line on four general geophysical signals: exponential function, periodic signal, and their hybrids. The exact signals, $f_i(t)$, in the time domain with their image functions, $F_i(s)$, in the Laplace domain are listed in Table 1. The relative errors using different parameters $\{a, m, N\}$ are analysed. Note that here, $N$ is the number of truncations of the image function series before series re-integration and the Euler's transform for acceleration are utilized.

Here, a sampling of time $t$ is used in the interval [1E−2, 15] with a constant step 1E−2 and $\tau_0 = 1.8$ and $\omega_0 = 2\pi/5$. Eqs (16) and (17) are thereafter employed to calculate an approximation of the inverse Laplace transform, $f_i^{amN}(t)$, from $F_i(s)$ by setting a list of values of parameters $\{a, m, N\}$. The maximum relative error of $f_i^{amN}(t)$ in the interval [1E−2, 15] is estimated by the following formula:

$$\max\left\{\left|\frac{f_i^{amN}(t) - f_i(t)}{f_i(t)}\right|,\ 0.01 < t < 15\right\}. \tag{27}$$

The maximum relative error of $f_i^{amN}(t)$ is calculated and plotted in Fig. 4. As shown in this figure, it is clear that the even number of $m$ and the large values of $a$ and $N$ result in sufficiently small errors for the four signals. The odd number of $m$, however, results in larger

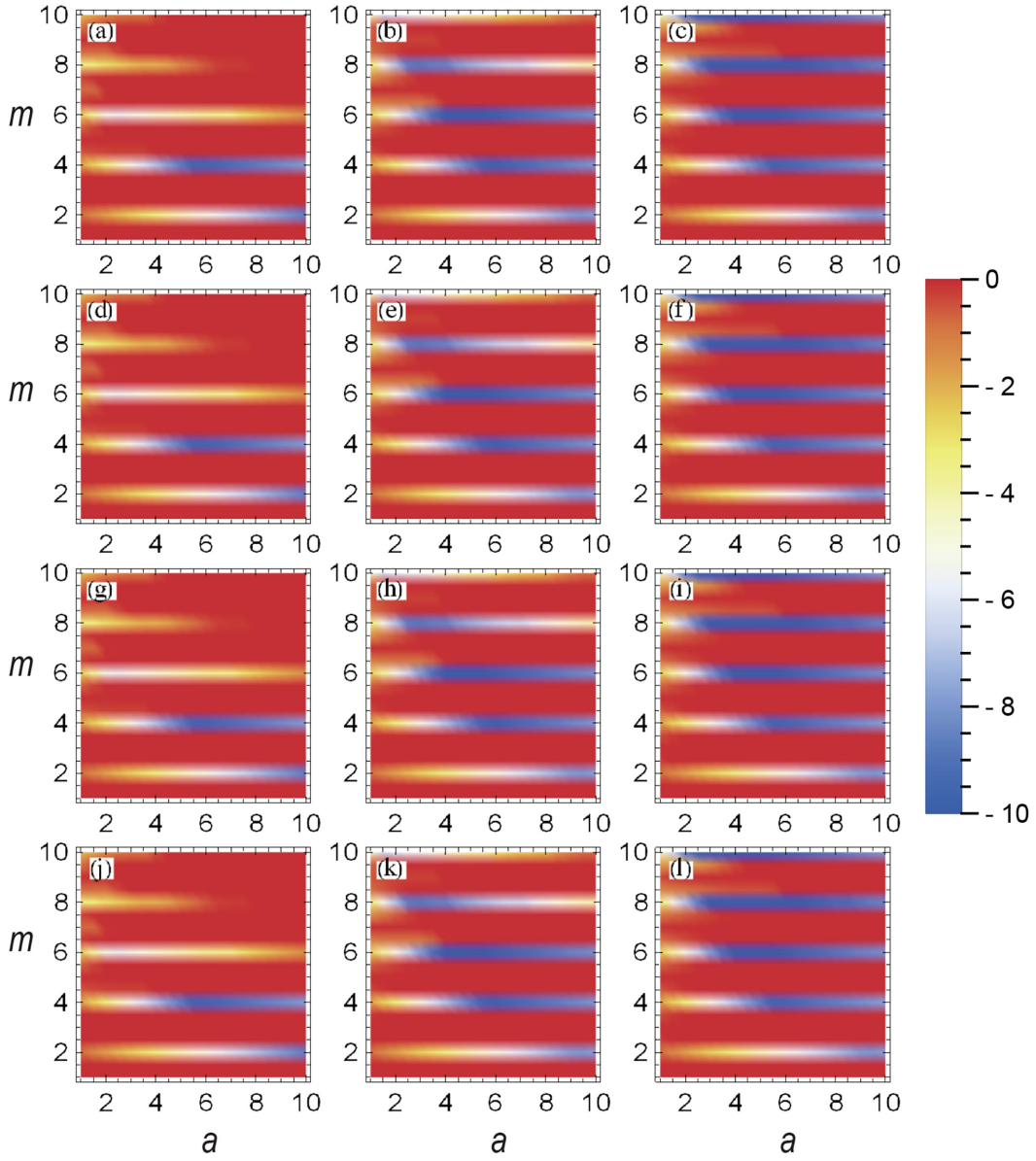


**Figure 4.** Maximum relative error of four signals calculated approximately by the proposed inverse Laplace transform method. The $i$th row for the signal $f_i$; the first, second and third columns for the terms of $N$ equals to 100, 200 and 400, respectively and the coloured value, $-j$, means $10^{-j}$ for the relative error.

relative errors. As a result, the horizontal stripes of large and small relative errors are shown in the Fig. 4. Although the value of $m$ can be a real number, not just an integer from eq. (7), the numerical analysis of relative error shows that the even value of $m$ will lead to a better performance in the proposed algorithm. The reason is that the even value of $m$ will result in a well-behaviour alternating and decreasing series through eqs (16) and (17) which can be effectively summed by the Euler's transform. So, only the even value of $m$ will be considered to obtain the optimized parameters in the following text. We also find that the value of $N$ only have a relatively weak impact on the relative errors for the four defined signals if hundreds sampling points is used during the summation process.

In Fig. 5, the mean relative errors of $f_i^{amN}(t)$—for the time in the interval [1E−2, 15] and using the terms of $N$ in the interval [100, 500]—are calculated and plotted. It is observed that the mean relative errors can be less than $10^{-6}$ if $m$ is equal to 4 and $a$ is greater than 5.

It can thus be concluded that for practical calculation, $m$ may be set to 4 and $a$ to approximately 6 (see the black cycle in Fig. 5). Moreover, approximately 100 terms of $F(s_k)$ are used to obtain the corresponding signals in the time domain with an extremely small relative error (approximately less than $10^{-6}$) for some common geophysical signals.

## 4. APPLICATION CASE OF IMPULSE LOAD LOVE ON VISCOELASTIC EARTH

To simulate the global viscoelastic deformations caused by the post-glacial rebound, the load Love numbers for a point source at the North pole should be calculated with high accuracy (e.g. Peltier 1974) in a viscoelastic Earth model. An essential step in the use of the correspondence principle is to derive the inverse Laplace transform of these complex Love numbers. The proposed method can be effectively applied for this geodynamic problem.

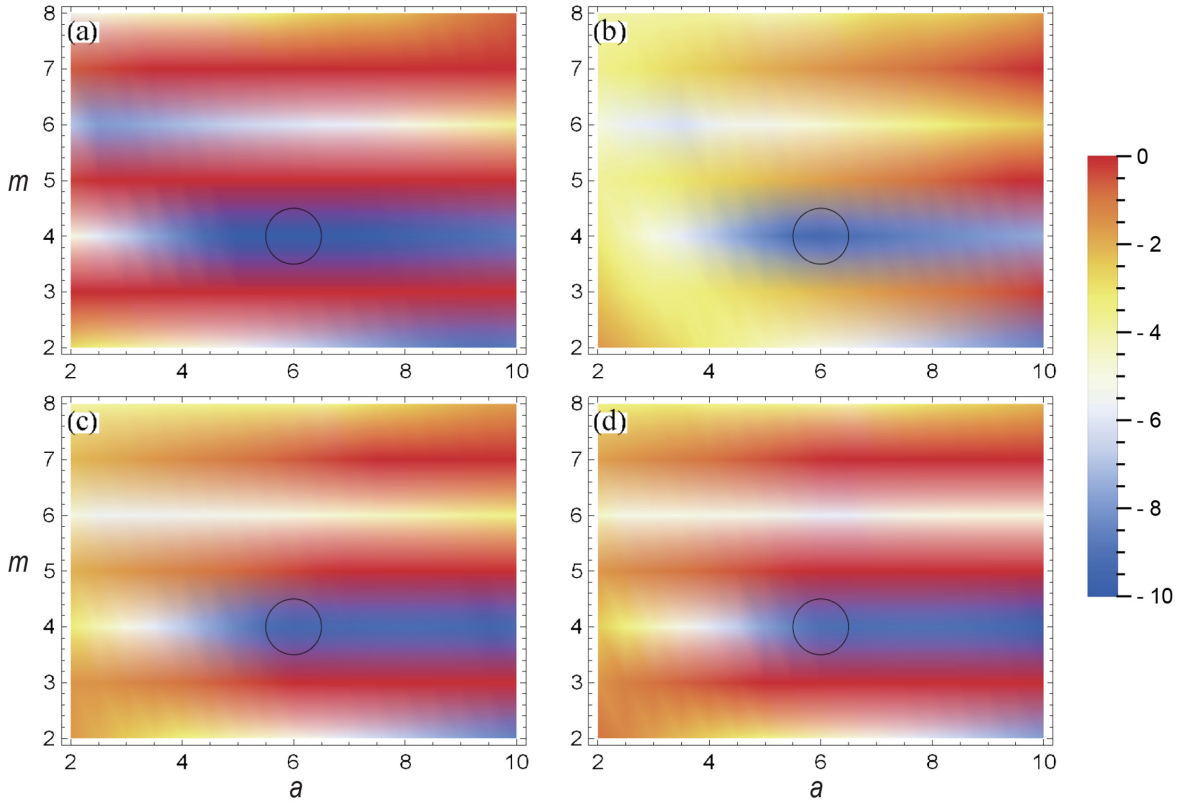


**Figure 5.** Mean relative errors of $f_i^{amN}(t)$ with different parameters of $\{a, m\}$ for the time in the interval [1E−2, 15] and for $N$ in the interval [100, 500]. The coloured value, $-j$, means $10^{-j}$; (a)–(d) for $f_1^{amN}$, $f_2^{amN}$, $f_3^{amN}$, $f_4^{amN}$), respectively. The point ($m = 6, a = 4$) is marked by a black circle.

**Table 2.** Parameters of the Earth model.

| Shear modulus, $\mu$ | Maxwell viscosity, $\eta$ | Mean radius, $R$ | Surface gravity, $g$ | Density, $\rho$ |
|---|---|---|---|---|
| $5 \times 10^{10}$ Pa | $1 \times 10^{19}$ Pa·s | $6371 \times 10^3$ m | 9.8 m s$^{-2}$ | $5.502 \times 10^3$ kg m$^{-3}$ |

Here, parameters $a$ and $m$ are set to 6 and 4, respectively, and 100 sampling terms of the image function for the proposed inverse Laplace transform are used. The analytical viscoelastic load Love numbers in a homogeneous, self-gravitating and incompressible Earth with a Maxwell rheology are approximated. For comparison, one of the three elastic load Love numbers, that is $k_n$, can be analytically calculated as

$$k_n = \frac{-1}{1 + M\alpha} \tag{28}$$

where $\alpha = \mu/(\rho g R)$ is the dimensionless shear modulus; $M = 2(n+2) + 3/n$ is the degree factor; $\mu$ is the elastic Lame parameter; $\rho$ is density; $R$ is the mean Earth radius; $g$ is surface gravity and $n$ is the harmonic degree. The correspondence principle ensures that the viscoelastic complex Love number is written as

$$k_n^V(s) = \frac{-1}{1 + M\tilde{\alpha}(s)}, \tilde{\alpha}(s) = \frac{s}{s + \mu/\eta}\alpha. \tag{29}$$

The temporal impulse Love number is

$$k_n^{\delta}(t) = \int_L k_n^V(s)\, e^{st} ds, \tag{30}$$

where $L$ is the Bromwich integral path. After the analytical integration, the impulse Love number, $k_n^{V\delta}(t)$, is expressed as

$$k_n^{V\delta}(t) = k_n\, \delta(t) + k_n^{\delta}(t), k_n^{\delta}(t) = \frac{-M\alpha}{(M\alpha+1)^2}\frac{\mu}{\eta} e^{\frac{-t\mu}{(M\alpha+1)\eta}}. \tag{31}$$

In the above expression, the impulse Love number contains two terms, the first one relating to the Dirac delta function and the second relating to an exponential function. For simplicity, the first term of the impulse Love number will be omitted. And the second term $k_n^{\delta}(t)$ is called impulse Love number hereafter.

Similarly, the Love number in the case of a Heaviside step loading force is calculated by

$$k_n^H(t) = \int_L k_n^V(s)\frac{e^{st}}{s} ds, \tag{32}$$

and after the analytical integration, the step loading Love number $k_n^H(t)$, is expressed as

$$k_n^H(t) = -1 + \frac{M\alpha}{M\alpha+1} e^{\frac{-t\mu}{(M\alpha+1)\eta}}. \tag{33}$$

Then, the impulse Love number, $k_n^{\delta}(t)$, and the step loading Love number, $k_n^H(t)$, are estimated by the viscoelastic complex Love number, $k_n^V(t)$, using the proposed inverse Laplace transform. The approximation of $k_n^{\delta}(t)$ and $k_n^H(t)$ is then written as $k_n^{A\delta}(t)$ and $k_n^{AH}(t)$, respectively. The parameter values of the Earth model are listed in Table 2. Both the relative and absolute errors of the impulse Love number and the step loading Love number are calculated and analysed in Figs 6 and 7.

As expected, the time-dependent $k$-Love number for the impulse loading force and a Heaviside step loading force calculated by the proposed inverse Laplace transform can be highly accurate with the

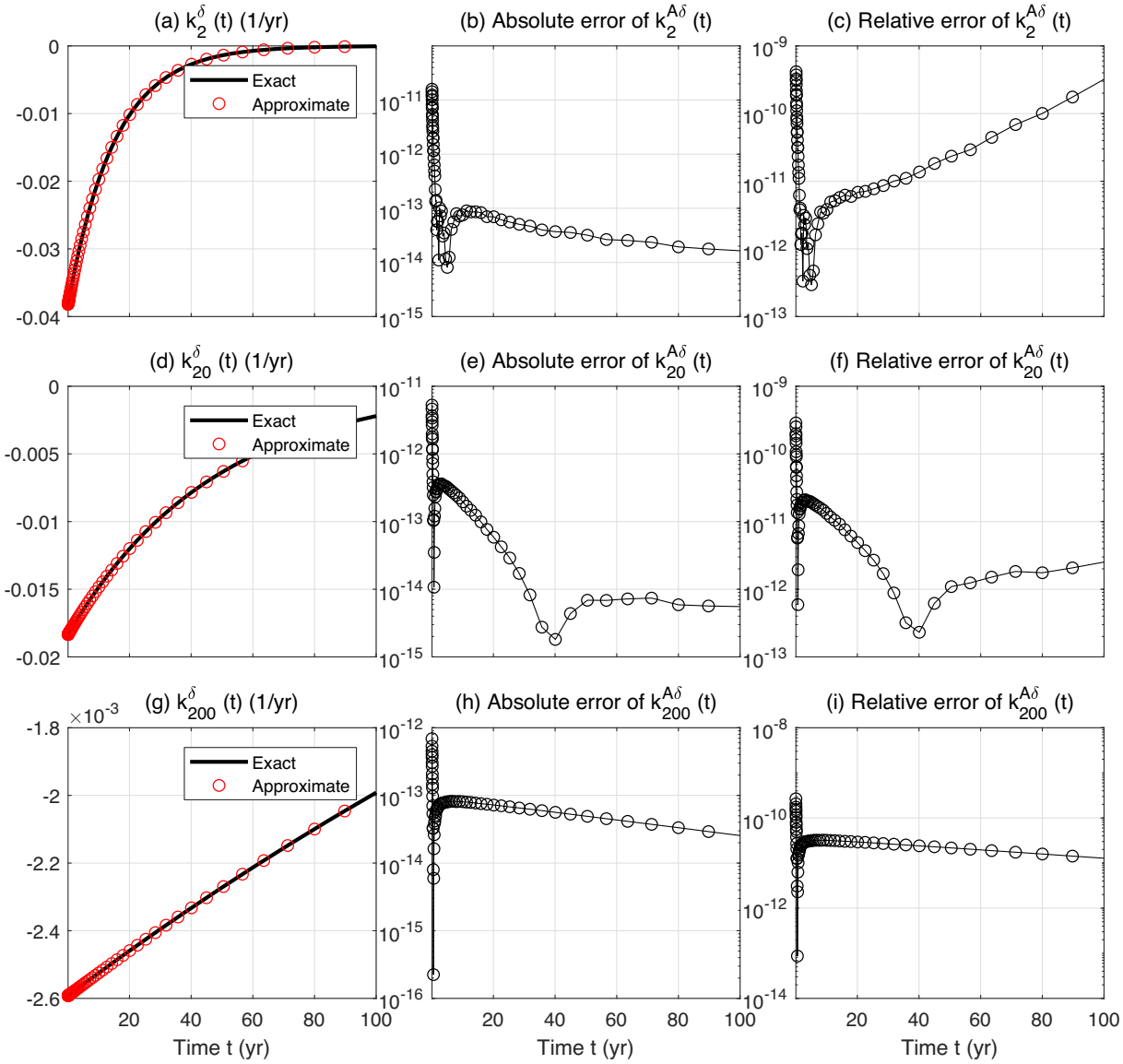


**Figure 6.** Comparison of the exact ($k_n^{\delta}(t)$, black lines) and approximate ($k_n^{A\delta}(t)$, red circles) impulse $k$-Love numbers (first column) calculated by analytical formula and approximate inverse Laplace transform, respectively. The second and third columns are the absolute and relative error of approximate impulse Love number, respectively. The first, second and third rows denotes $k$-Love number with degree 2, degree 20 and degree 200, respectively.

relative and absolute errors less than $10^{-6}$ using 100 terms of the complex Love numbers.

## 5 DISCUSSION AND CONCLUSIONS

A numerical algorithm that is effective for an inverse integral transform, such as the Laplace transform, is considered as one of the key mathematical steps for accurately implementing geodynamic simulations. The optimized approximate inverse Laplace transform proposed in this paper can be directly employed to compute geo-deformations in the viscoelastic Earth model for many practical problems. Compared with a previous study (Tang & Sun 2019), the proposed approximate method has a shorter subprocess, a higher accuracy and approximately the same computational overhead. Specifically, the integral kernel is directly approximated as a rational function with two adjustable parameters; thereafter, the residual of the integrand is applied, and the final similar formula is derived as a series summations at certain special points. The geometric meaning of the two permeates in this series formula is considerably clear: the location of the sampling points in the complex plane is at $a/t + 2\pi i/(mt)$. On the other hand, the proposed method can be explained from another perspective: the implementation of the inverse Laplace transform may not be necessary from the exact image function, $F(s)$; instead, the original function, $f(t)$, is estimated from the approximated image function, $F(s)/(1 - \mathrm{e}\hat{}(m(st - a))$. The proposed method can be treated as an exact inverse Laplace transform formula of the approximated image function. In fact, the image function is usually obtained by numerical calculations and may contain computational errors. The further approximation of the image function is therefore a distinct and intuitive operation. Remarkably, this type of approximation results in a considerably simple expression of the original function, that is a weighted series summation of the image function at certain

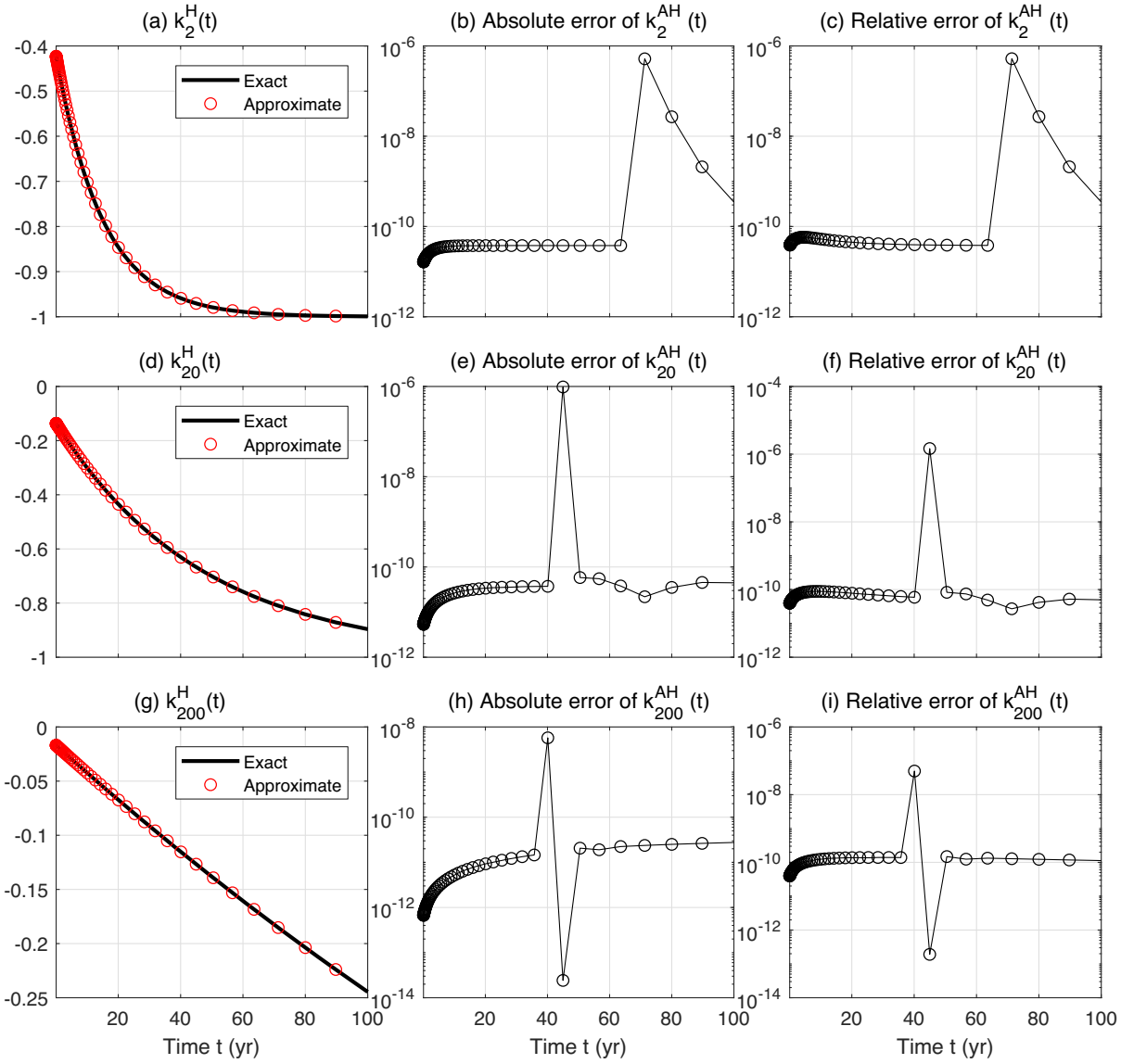


**Figure 7.** Similar to Fig. 6, but for the step loading Love numbers $k_n^H(t)$ and $k_n^{AH}(t)$.

special points. The key idea may be employed for other integral transforms.

From a mathematical point of view, the inverse Laplace transform is an inherently ill-posed problem. Four groups of algorithms have been time-tested (Abate & Valko 2004) to treat this type of problem: (i) Fourier series expansion, (ii) Laguerre function expansion, (iii) combination of Gaver functions and (iv) deformed Bromwich contour. The proposed method in this paper can be classified into the fourth category but with an approximation of the integral kernel. Each algorithm clearly has its own special feature on computational effectiveness. The requirements of the computing environment, the number of sampling points necessary, the computational error and the applicability to various practical physical problems differ among these algorithms.

In this paper, the proposed method is implemented through a particular example for the exponential function, periodic function and their combination. The absolute and relative errors of the approximated calculated original function is less than $10^{-6}$ when the parameters are $a = 6$ and $m = 4$, and approximately 100 sampling terms of the image function are employed to accelerate the series convergence following an Euler's transformation. It can thus be concluded that the extended and optimized approach of the approximate inverse Laplace transform (Valsa & Brancik 1998; Tang & Sun 2019) has a better performance, that is having a lower relative error of the transformed functions and an approximately the same required terms of the image function. The systematic and detailed comparison with other calculation methods, such as Weeks method (a specific branch of the Laguerre function expansion), will be left for a future study.

From the perspective of practical geophysical applications, the proposed method can also be widely employed as other mature approaches, such as the closed-path numerical integration (Tanaka *et al*. 2006, 2007), with the same or better computational efficiency. It can be applied not only for investigating post-seismic relaxation

deformations (e.g. Gautam *et al.* 2019; Cambiotti 2020) and post-glacial rebound deformations but also for other geodynamic simulations, such as the penetrating fluid problem (e.g. Kuo *et al.* 2011) and global mantle convection (e.g. Edwards 2019).

## ACKNOWLEDGEMENTS

We greatly appreciate the constructive comments by the Editor (Prof. Bert Vermeersen), and two anonymous reviewers, which have greatly improved the manuscript. This research was supported financially by the National Natural Science Foundation of China (41774088, 41974093, 41331066 and 41474059), the Key Research Program of Frontier Sciences, Chinese Academy of Sciences (QYZDY-SSWSYS003). The authors are grateful to Jonas Lundgren for kindly providing an effective MATLAB code for the implementation of Euler's transform. The data are available in a public research repository on Zenodo (https://doi.org/10.5281/zenodo.3903980).

## REFERENCES

Abate, J. & Valko, P.P., 2004. Multi-precision laplace transform inversion, *Int. J. Numer. Methods Eng.,* **60,** 979–993.

Cambiotti, G., 2020. Joint estimate of the coseismic 2011 Tohoku earthquake fault slip and post-seismic viscoelastic relaxation by GRACE data inversion, *Geophys. J. Int.,* **220,** 1012–1022.

Cambiotti, G., Barletta, V.R., Bordoni, A. & Sabadini, R., 2009. A comparative analysis of the solutions for a Maxwell Earth: the role of the advection and buoyancy force, *Geophys. J. Int.,* **176,** 995–1006.

Cambiotti, G., Klemann, V. & Sabadini, R., 2013. Compressible viscoelastodynamics of a spherical body at long timescales and its isostatic equilibrium, *Geophys. J. Int.,* **193,** 1071–1082.

Cambiotti, G. & Sabadini, R., 2010. The compressional and compositional stratifications in Maxwell earth models: the gravitational overturning and the long-period tangential flux, *Geophys. J. Int.,* **180,** 475–500.

Edwards, M.R., 2019. Deep mantle plumes and an increasing Earth radius, *Geod. Geodyn.,* **10,** 173–178.

Farrell, W.E., 1972. Deformation of the Earth by surface loads, *Rev. Geophys. Space Phys.,* **10,** 761–797.

Gautam, P.K., Sathyaseelan, R., Pappachen, J.P., Kumar, N., Biswas, A., Philip, G., Dabral, C.P. & Pal, S.K., 2019. GPS measured static and kinematic offsets at near and far field of the 2011 Mw 9.0 Tohoku-Oki earthquake, *Geod. Geodyn.,* **10,** 213–227.

Kuo, C.C., Huang, C.S. & Yeh, H.D., 2011. Transient analysis for fluid injection into a dome reservoir, *Adv. Water Resour.,* **34,** 1553–1562.

Melini, D., Cannelli, V., Piersanti, A. & Spada, G., 2008. Post-seismic rebound of a spherical Earth: new insights from the application of the Post-Widder inversion formula, *Geophys. J. Int.,* **174,** 672–695.

Ozawa, S., Nishimura, T., Suito, H., Kobayashi, T., Tobita, M. & Imakiire, T., 2011. Coseismic and postseismic slip of the 2011 magnitude-9 Tohoku-Oki earthquake, *Nature,* **475,** 373–376.

Peltier, W.R., 1974. The impulse response of a Maxwell Earth, *Rev. Geophys.,* **12,** 649–669.

Piersanti, A., Spada, G., Sabadini, R. & Bonafede, M., 1995. Global post-seismic deformation, *Geophys. J. Int.,* **120,** 544–566.

Pollitz, F.F., 1992. Postseismic relaxation theory on the spherical Earth, *Bull. seism. Soc. Am.,* **82,** 422–453.

Pollitz, F.F., 1997. Gravitational viscoelastic postseismic relaxation on a layered spherical Earth, *J. geophys. Res.—Solid Earth,* **102,** 17921–17941.

Pollitz, F.F., Bürgmann, R. & Banerjee, P., 2006. Post-seismic relaxation following the great 2004 Sumatra-Andaman earthquake on a compressible self-gravitating Earth, *Geophys. J. Int.,* **167,** 397–420.

Sabadini, R., Yuen, D.A. & Boschi, E., 1984. The effects of post-seismic motions on the moment of inertia of a stratified viscoelastic Earth with an asthenosphere, *Geophys. J. R. astr. Soc.,* **79,** 727–745.

Spada, G. & Boschi, L., 2006. Using the Post-Widder formula to compute the Earth's viscoelastic Love numbers, *Geophys. J. Int.,* **166,** 309–321.

Sun, W. & Okubo, S., 1993. Surface potential and gravity changes due to internal dislocations in a spherical earth-I. Theory for a point dislocation, *Geophys. J. Int.,* **114,** 569–592.

Sun, W. & Okubo, S., 2002. Surface potential and gravity changes due to internal dislocations in a spherical earth-II. Application to a finite fault, *Geophys. J. Int.,* **132,** 79–88.

Tanaka, Y., Okuno, J. & Okubo, S., 2006. A new method for the computation of global viscoelastic post-seismic deformation in a realistic earth model (I)—vertical displacement and gravity variation, *Geophys. J. Int.,* **164,** 273–289.

Tanaka, Y., Okuno, J. & Okubo, S., 2007. A new method for the computation of global viscoelastic post-seismic deformation in a realistic earth model (II)—horizontal displacement, *Geophys. J. Int.,* **170,** 1031–1052.

Tang, H., Dong, J., Zhang, L. & Sun, W., 2020. Deformation of a spherical, viscoelastic, and incompressible Earth for a point load with periodic time change, *Geophys. J. Int.,* **222,** 1909–1922.

Tang, H. & Sun, W.K., 2018. Closed-form expressions of seismic deformation in a homogeneous Maxwell Earth model, *J. geophys. Res.—Solid Earth,* **123,** 6033–6051.

Tang, H. & Sun, W.K., 2019. New method for computing postseismic deformations in a realistic gravitational viscoelastic Earth model, *J. geophys. Res.—Solid Earth,* **124,** 5060–5080.

Valsa, J. & Brancik, L., 1998. Approximate formulae for numerical inversion of Laplace transforms, *Int. J. Numer. Model.—Electr. Netw. Devices Fields,* **11,** 153–166.

Vermeersen, L.L.A. & Sabadini, R., 1997. A new class of stratified viscoelastic models by analytical techniques, *Geophys. J. Int.,* **129,** 531–570.

Vermeersen, L.L.A., Sabadini, R. & Spada, G., 1996. Compressible rotational deformation, *Geophys. J. Int.,* **126,** 735–761.

Wang, R., Lorenzo-Martín, F. & Roth, F., 2006. PSGRN/PSCMP—a new code for calculating co- and post-seismic deformation, geoid and gravity changes based on the viscoelastic-gravitational dislocation theory, *Comput. Geosci.,* **32,** 527–541.